The Journal of Engineering

The 7th International Conference on Renewable Power Generation (RPG 2018)

IET Journals
The Institution of Engineering and Technology

Dynamic modelling of grid-connected permanent magnet synchronous generator wind turbine: rectifier dynamics and control design

eISSN 2051-3305
Received on 5th November 2018
Accepted on 10th January 2019
doi: 10.1049/joe.2018.9343
www.ietdl.org

Muhammad Ammar Ahmed[1] ✉, *Tuomas Messo*[1], *Paavo Rasilo*[1], *Jenni Rekola*[1]

[1]*Laboratory of Electrical Energy Engineering, Tampere University of Technology, P.O. Box 692, FI-33101 Tampere, Finland*

✉ *E-mail: muhammad.ahmed@tuni.fi*

Abstract: Wind energy technology is developing more and more from recent decades in many countries. Therefore, addressing the latest wind turbine research issues, this study develops a dynamic model of a permanent magnet synchronous generator and an active rectifier—as part of a unified dynamic model of a wind turbine generator in MATLAB/Simulink. In addition, a novel technique for the verification of the open-loop and the closed-loop transfer functions in the frequency domain is presented. The technique develops by analysing the frequency responses of the transfer function at various frequencies. Furthermore, the cascaded control loops of the developed model are designed and the stability of the designed controllers is tested in response to step changes in reference values.

1 Introduction

During the late 19th and early 20th century, the concept of electric power generation through wind energy has increased significantly [1]. Throughout the whole 20th century, wind technology was improved step by step until the 1990s, when there was a boom of sustainable energy resources all around the world especially in wind power. Few of the major reasons for this global trend could be the increasingly negative effects of global warming and increasing oil price [1].

Compared with other forms of renewable energy resources, wind power is increased drastically during the last few decades especially in Europe, North America and China. For example, during the year 2017, the additional wind power capacity installed in Europe is 16.8 GW, which is 25% more than the year 2016. This made wind power the second largest form of power generation in Europe (total net installed capacity is 169 GW) after gas power generation [2].

There are various types of conversion solutions developed to maximise the energy conversion efficiency in wind power, however, the two-level AC–DC–AC conversion between the generator and the load is widely adopted [3]. Although wind power technology has been significantly developed all over the world, there are certain issues that still need to be addressed to improve the overall energy efficiency of a wind turbine [4]. Therefore, the emphasis of this research work is the development of the control design of the permanent magnet synchronous generator (PMSG) and the power electronics involved in the wind turbine and determine the issues involved in the overall performance. PMSG mechanism is comparatively simple and it does not require any separate electrical excitation [3, 5]. In addition, their performance is highly reliable with minimum maintenance required; therefore, these generators are widely used in low speed, high power wind turbines [6].

According to a report published by the IEC committee, one of the major obstacles in developing better control algorithms is the lack of a unified dynamic model of a wind turbine [7]. Therefore, approaching towards the ultimate goal of designing such a model—as shown in Fig. 1—this study develops the dynamic model of the PMSG and the rectifier stage. Thus, providing useful tools to design a stable and robust control system in a deterministic way.

The dynamic model produces 16 transfer functions between different input and output variables, which can be verified using frequency-response analysis (FRA). In this study, the model is verified from a Simulink switching model in open-loop and closed-loop including cascaded control loop gains.

The dynamic model is shown to predict the true control-related transfer functions with excellent accuracy, allowing the robust design of the cascaded control structure. In fact, there seems to be a lack of verified dynamic models for PMSG wind turbine rectifier in the literature [3, 8, 9].

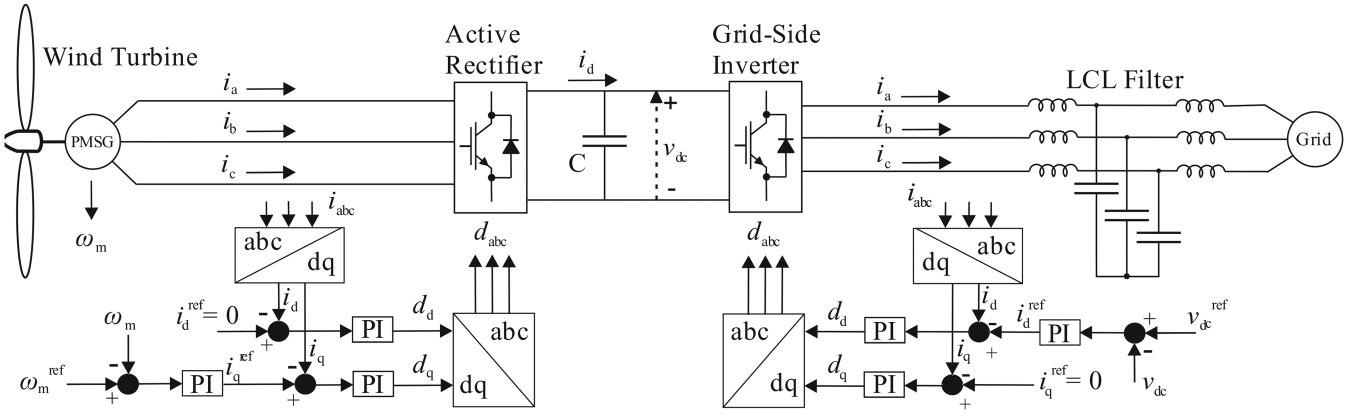

Fig. 1 *Depiction of full-scale wind power generation unit with a control system*

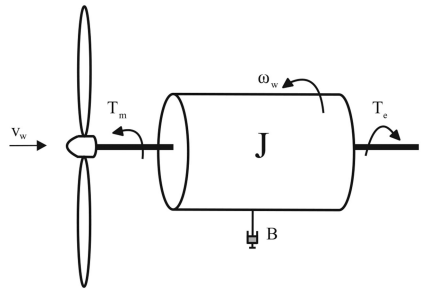

Fig. 2 *Equivalent mechanical circuit of the equation of motion and the wind turbine*

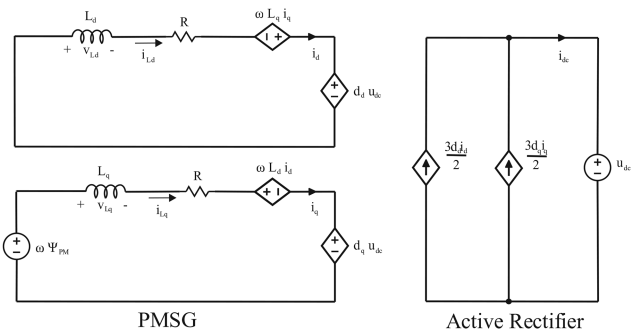

Fig. 3 *Equivalent electrical circuit of the PMSG and the active rectifier*

The paper is organised as follows. The first section develops the dynamic (or small-signal) model of the PMSG generator and the rectifier. The second section demonstrates how the dynamic model is employed in successful control design. The dynamic model is further verified in section three by means of FRA. In the final section of the paper, the control design results are presented.

2 Mathematical modelling

2.1 Wind turbine model

The wind power is converted into mechanical power of the wind turbine shaft in the form of mechanical torque T_m and expressed as

$$T_\mathrm{m} = \frac{1}{2}\rho A_\mathrm{r} C_\mathrm{p}(\lambda,\beta)\frac{v_\mathrm{w}^3}{\omega_\mathrm{m}}, \tag{1}$$

where ρ is the air density, A_r is the area swept by the rotor, β is the blade angle which remains zero in this case, v_w is the wind speed, ω_m is the rotor angular speed and λ is the tip speed ratio, which is equal to

$$\lambda = \frac{\omega_\mathrm{m} r}{v_\mathrm{w}}. \tag{2}$$

The turbine power coefficient C_p is a non-linear function of tip-speed ratio λ and blade pitch angle β, however, since $\beta = 0°$, then the C_p can be mathematically expressed as [9]

$$C_\mathrm{p}(\lambda) = \frac{1}{2}\left(\frac{98}{\lambda_i} - 5\right)\mathrm{e}^{(-16.5/\lambda_i)}, \tag{3}$$

$$\frac{1}{\lambda_i} - \left(\frac{1}{\lambda + 0.089} - 0.035\right). \tag{4}$$

The electromagnetic torque T_e is produced in response to the mechanical torque T_m in the PMSG, which can be defined as [3]

$$T_\mathrm{e} = \frac{3}{2}p\left(\Psi_\mathrm{PM}\langle i_{Lq}\rangle - (L_d - L_q)\langle i_{Ld}\rangle\langle i_{Lq}\rangle\right), \tag{5}$$

where p is the number of pole pairs of PMSG, Ψ_PM is the stator flux linkage caused by the permanent magnets, L_d and L_q are the d-axis and q-axis generator inductances, i_{Ld} and i_{Lq} are the d-axis and q-axis PMSG currents, respectively. The equation of motion for the PMSG is [3]

$$\begin{aligned} J\frac{\mathrm{d}\omega_\mathrm{m}}{\mathrm{d}t} &= T_\mathrm{m} - B\omega_\mathrm{m} - T_\mathrm{e}, \\ J\frac{\mathrm{d}\omega_\mathrm{m}}{\mathrm{d}t} &= T_\mathrm{m} - B\omega_\mathrm{m} - \frac{3}{2}p\left(\Psi_\mathrm{PM}\langle i_{Lq}\rangle - (L_d - L_q)\langle i_{Ld}\rangle\langle i_{Lq}\rangle\right), \end{aligned} \tag{6}$$

where J is the moment of inertia on the PMSG shaft and B is the damping constant. The mechanical representation of the wind turbine model described in (1)–(6), is shown in Fig. 2.

2.2 PMSG and rectifier model

To develop the dynamic model of the PMSG and the rectifier, two-phase dq frame of reference is used, in which q-axis leads d-axis by 90° [6]. The stator voltages of PMSG can be defined in the dq-domain using the following equations considering the currents to be flowing out of the generator [8]

$$\begin{cases} \langle v_d\rangle = -R\langle i_{Ld}\rangle + \omega_\mathrm{e} L_q\langle i_{Lq}\rangle - L_d\dfrac{\mathrm{d}\langle i_{Ld}\rangle}{\mathrm{d}t}, \\ \langle v_q\rangle = -R\langle i_{Lq}\rangle - \omega_\mathrm{e} L_d\langle i_{Ld}\rangle - L_q\dfrac{\mathrm{d}\langle i_{Lq}\rangle}{\mathrm{d}t} + \omega_\mathrm{e}\Psi_\mathrm{PM}, \\ L_d\dfrac{\mathrm{d}\langle i_{Ld}\rangle}{\mathrm{d}t} = -d_\mathrm{d}\langle v_\mathrm{dc}\rangle - R\langle i_{Ld}\rangle + p\omega_\mathrm{m} L_q\langle i_{Lq}\rangle, \\ L_q\dfrac{\mathrm{d}\langle i_{Lq}\rangle}{\mathrm{d}t} = -d_\mathrm{q}\langle v_\mathrm{dc}\rangle - R\langle i_{Lq}\rangle - p\omega_\mathrm{m} L_q\langle i_{Ld}\rangle + \Psi_\mathrm{PM} p\omega_\mathrm{m}, \end{cases} \tag{7}$$

where $\langle v_{d,q}\rangle = d_{d,q}\langle v_\mathrm{dc}\rangle$, $\omega_\mathrm{e} = p\omega_\mathrm{m}$ is the electrical rotor speed, R is the PMSG stator resistance, v_dc is the DC-link voltage and d_d and d_q are the modulation ratio d and q components.

In addition, the DC-current i_dc generated by the rectifier needs to be such that the AC and DC powers are equal as shown in Fig. 3. The DC-current is

$$i_\mathrm{dc} = \frac{3}{2}\left(d_d i_d + d_q i_q\right). \tag{8}$$

The equivalent electrical circuit of the PMSG and the rectifier model expressed in (7) and (8) is shown in Fig. 3.

2.3 Steady-state operating points

MATLAB/Simulink is used to verify the equations defined above by simulating the model first in open-loop and then in closed-loop. The steady-state operating point in obtained by setting the time derivative in (1)–(8) equals to zero, whereas, capital letters of inductor currents d- and q-component I_{Ld}, I_{Lq}, duty ratios d- and q-component D_d, D_q, DC-link voltage V_dc and PMSG mechanical speed Ω_m are used to denote the corresponding steady state values.

Since the PMSG used in this work is a salient generator, therefore the stator inductance L_d is not equal to L_q [10]. However, the control design is done according to non-salient PMSG that means $L_d = L_q$, hence, the assumed value of d-axis generator current $I_{Ld} = 0$. In addition, wind speed $v_\mathrm{w} = 10$ m/s and the nominal speed of the generator is set to $\Omega_\mathrm{m} = 13.299$ rad/s. With this assumption, the mechanical torque T_m value can be calculated from (1) keeping lambda to its optimum value $\lambda_\mathrm{opt} = 6.31$. Other known steady-state variables along with their parameter values are mentioned in Table 1. From (5) and (6)

$$I_{Lq} = \frac{2}{3}\cdot\frac{(T_\mathrm{m} - B\Omega_\mathrm{m})}{p\Psi_\mathrm{PM}}. \tag{9}$$

Furthermore, duty-ratio q-axis D_q is solved from the inductor current q-axis I_{Lq} from (7) and (9) as

$$D_q = \frac{\Psi_{\mathrm{PM}} p\Omega_{\mathrm{m}} - RI_{Lq} - p\Omega_{\mathrm{m}} L_d I_{Ld}}{V_{\mathrm{dc}}} = \frac{\Psi_{\mathrm{PM}} p\Omega_{\mathrm{m}} - RI_{Lq}}{V_{\mathrm{dc}}}. \quad (10)$$

Similarly from (7) and $I_{Ld} = 0$, duty-ratio d-axis D_d is solved as

$$D_d = \frac{p\Omega_{\mathrm{m}} L_q L_{Lq}}{V_{\mathrm{dc}}}. \quad (11)$$

2.4 Linearisation

The averaged state-space model from (6)–(8) is linearised to a specific operating point by taking the partial derivative of input, output and state variables. The cap sign $\hat{x}$ denotes the small-signal variable.

$$\begin{aligned}
\frac{\mathrm{d}\hat{i}_{Ld}}{\mathrm{d}t} &= -\frac{R}{L_d}\hat{i}_{Ld} + \frac{p\Omega_{\mathrm{m}} L_q}{L_d}\hat{i}_{Lq} \\
&\quad + \frac{pL_q L_{Lq}}{L_d}\hat{\omega}_{\mathrm{m}} - \frac{D_d}{L_d}\hat{v}_{\mathrm{dc}} - \frac{V_{\mathrm{dc}}}{L_d}\hat{d}_d, \\
\frac{\mathrm{d}\hat{i}_{Lq}}{\mathrm{d}t} &= -p\Omega_{\mathrm{m}}\frac{L_d}{L_q}\hat{i}_{Ld} - \frac{R}{L_q}\hat{i}_{Lq} \\
&\quad - \left(p\frac{L_d}{L_q}I_{Ld} - \frac{\Psi_{\mathrm{PM}} p}{L_q}\right)\hat{\omega}_{\mathrm{m}} - \frac{D_q}{L_q}\hat{v}_{\mathrm{dc}} - \frac{V_{\mathrm{dc}}}{L_q}\hat{d}_q, \\
\frac{\mathrm{d}\hat{\omega}_{\mathrm{m}}}{\mathrm{d}t} &= \frac{3}{2}\frac{p(L_d - L_q)I_{Lq}}{J}\hat{i}_{Ld} \\
&\quad - \frac{3}{2}\frac{p(\Psi_{\mathrm{PM}} - (L_d - L_q)I_{Ld})}{J}\hat{i}_{\mathrm{Lq}} - \frac{B}{J}\hat{\omega}_{\mathrm{m}} + \frac{1}{J}\hat{\tau}_{\mathrm{m}}, \\
\hat{i}_{\mathrm{dc}} &= \frac{3}{2}D_d\hat{i}_{Ld} + \frac{3}{2}D_q\hat{i}_{Lq} + \frac{3}{2}I_{Ld}\hat{d}_d + \frac{3}{2}I_{Lq}\hat{d}_q.
\end{aligned} \quad (12)$$

Furthermore, the linearised state-space equations can be formulated as linearised state matrices (see (13)) . In order to tune the controllers for the wind turbine model, the transfer functions between input and output variables need to be obtained. This can be done by taking the Laplace-transformation of the linearised matrices of (13)

Table 1 Parameters of PMSG and rectifier

Parameters	Numerical values
air density ρ	1.125 kg/m^3
damping constant B	0 Nm/(rad/s)
DC-link voltage v_{dc}	700 V
generator pole pairs p	6
moment of inertia J	1495 kg m^2
permanent magnet flux linkage Ψ_{PM}	3.1851 Wb
radius of turbine blades r	4.75 m
stator inductance d-component L_d	0.057 H
stator inductance q-component L_q	0.072 H
stator resistance R	1.0463 Ω
wind speed v_{w}	10 m/s

$$\begin{bmatrix} \hat{i}_{Ld} \\ \hat{i}_{Lq} \\ \hat{\omega}_{\mathrm{m}} \\ \hat{i}_{\mathrm{dc}} \end{bmatrix} = \begin{bmatrix} G_{\tau-\mathrm{d}-\mathrm{o}} & G_{\mathrm{dc}-\mathrm{Ld}-\mathrm{o}} & G_{\mathrm{cL}-\mathrm{dd}-\mathrm{o}} & G_{\mathrm{cL}-\mathrm{qd}-\mathrm{o}} \\ G_{\tau-\mathrm{q}-\mathrm{o}} & G_{\mathrm{dc}-\mathrm{Lq}-\mathrm{o}} & G_{\mathrm{cL}-\mathrm{dq}-\mathrm{o}} & G_{\mathrm{cL}-\mathrm{qq}-\mathrm{o}} \\ G_{\tau-\omega-\mathrm{o}} & G_{\mathrm{dc}-\omega-\mathrm{o}} & G_{\mathrm{c}\omega-\mathrm{d}-\mathrm{o}} & G_{\mathrm{c}\omega-\mathrm{q}-\mathrm{o}} \\ G_{\tau-\mathrm{dc}-\mathrm{o}} & -Y_{\mathrm{o}-\mathrm{o}} & G_{\mathrm{dc}-\mathrm{dc}-\mathrm{o}} & G_{\mathrm{q}-\mathrm{dc}-\mathrm{o}} \end{bmatrix} \begin{bmatrix} \hat{\tau}_{\mathrm{m}} \\ \hat{v}_{\mathrm{dc}} \\ \hat{d}_d \\ \hat{d}_q \end{bmatrix}. \quad (14)$$

Transfer functions are taken from input duty-ratios $\hat{d}_d$, $\hat{d}_q$ and output variables $\hat{i}_{Ld}$, $\hat{i}_{Lq}$ and $\hat{\omega}_{\mathrm{m}}$ are important because these transfer functions play an important role in the control strategy of the designed model.

3 Verifications and control design

3.1 Open-loop transfer functions

Before implementing the control design, it is important to verify the transfer functions that take part in the control strategy. The dynamic model is verified in open-loop—with constant load torque—by injecting sinusoidal signals of different frequencies to the input signal. The output response is then compared with the input in the frequency domain to verify the transfer function. The Simulink setup for the open-loop verification is shown in Fig. 4.

Since the transfer functions from $\hat{d}_d$, $\hat{d}_q$ to $\hat{i}_{Ld}$, $\hat{i}_{Lq}$ and $\hat{\omega}_{\mathrm{m}}$ are taking part in the control design, the FRA results of only these ones are shown in Fig. 5.

From the figure, the dotted lines are the mathematical model of the transfer functions and their frequency response at various frequencies are depicted by small circles. As shown, the experimental values exactly match their corresponding mathematical values.

$$\begin{aligned}
\frac{\mathrm{d}}{\mathrm{d}t}\begin{bmatrix} \hat{i}_{Ld} \\ \hat{i}_{Lq} \\ \hat{\omega}_{\mathrm{m}} \end{bmatrix} &= \begin{bmatrix} -\frac{R}{L_d} & \frac{p\Omega_{\mathrm{m}} L_q}{L_d} & \frac{p\Omega_q L_q}{L_d} \\ -p\Omega_{\mathrm{m}}\frac{L_d}{L_q} & -\frac{R}{L_q} & -\left(p\frac{L_d}{L_q}I_{Ld} - \frac{\Psi_{\mathrm{PM}} p}{L_q}\right) \\ \frac{3}{2}\frac{p(L_d - L_q)I_{Lq}}{J} & -\frac{3}{2}\frac{p(\Psi_{\mathrm{PM}} - (L_d - L_q)I_{Ld})}{J} & -\frac{B}{J} \end{bmatrix} \\
&\quad + \begin{bmatrix} 0 & -\frac{D_d}{L_d} & -\frac{V_{\mathrm{dc}}}{L_d} & 0 \\ 0 & -\frac{D_q}{L_q} & 0 & -\frac{V_{\mathrm{dc}}}{L_q} \\ \frac{1}{J} & 0 & 0 & 0 \end{bmatrix} \begin{bmatrix} \hat{\tau}_{\mathrm{m}} \\ \hat{v}_{\mathrm{dc}} \\ \hat{d}_d \\ \hat{d}_q \end{bmatrix},
\end{aligned} \quad (13)$$

$$\begin{bmatrix} \hat{i}_{Ld} \\ \hat{i}_{Lq} \\ \hat{\omega}_{\mathrm{m}} \\ \hat{i}_{\mathrm{dc}} \end{bmatrix} = \begin{bmatrix} 1 & 0 & 0 \\ 0 & 1 & 0 \\ 0 & 0 & 1 \\ \frac{3}{2}D_d & \frac{3}{2}D_q & 0 \end{bmatrix} \begin{bmatrix} \hat{i}_{Ld} \\ \hat{i}_{Lq} \\ \hat{\omega}_{\mathrm{m}} \end{bmatrix} + \begin{bmatrix} 0 & 0 & 0 & 0 \\ 0 & 0 & 0 & 0 \\ 0 & 0 & 0 & 0 \\ 0 & 0 & \frac{3}{2}I_{Ld} & \frac{3}{2}I_{Lq} \end{bmatrix} \begin{bmatrix} \hat{\tau}_{\mathrm{m}} \\ \hat{v}_{\mathrm{dc}} \\ \hat{d}_d \\ \hat{d}_q \end{bmatrix}.$$

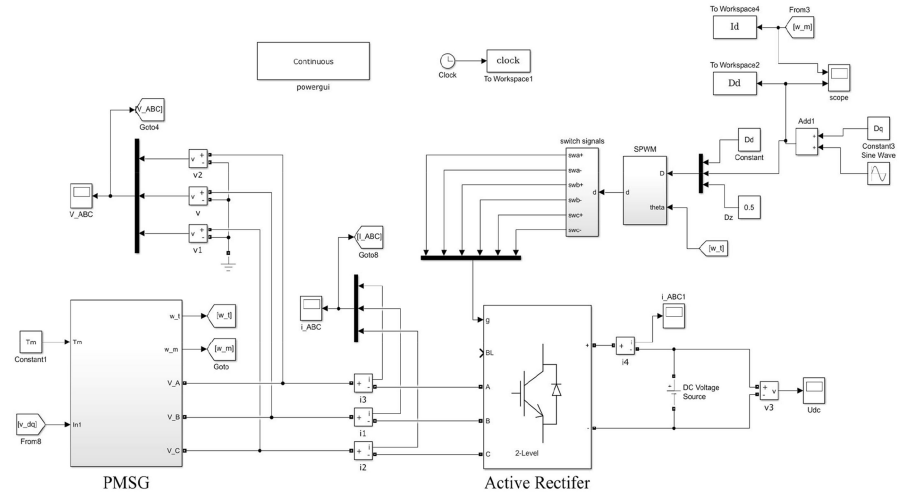

Fig. 4 *PMSG-rectifier Simulink switched model with sinusoidal perturbation to an input variable*

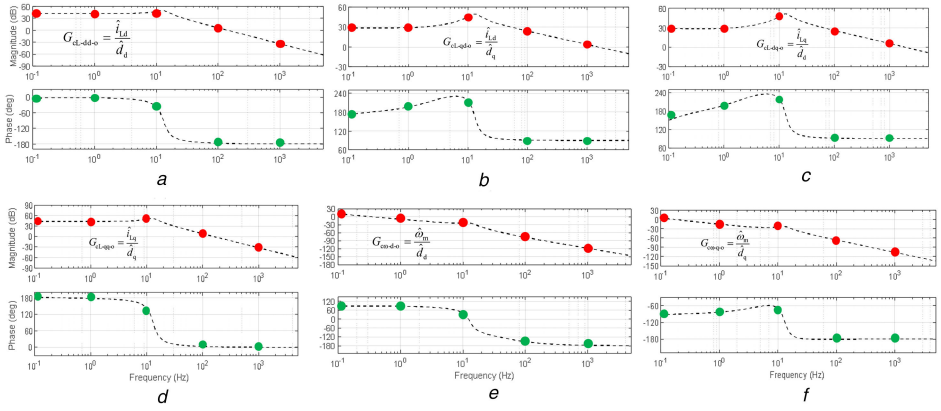

Fig. 5 *Frequency response analysis of open-loop transfer functions*
(a) $G_{\mathrm{cL\text{-}dd\text{-}o}}$, ***(b)*** $G_{\mathrm{cL\text{-}qd\text{-}o}}$, ***(c)*** $G_{\mathrm{cL\text{-}dq\text{-}o}}$, ***(d)*** $G_{\mathrm{cL\text{-}qq\text{-}o}}$, ***(e)*** $G_{\mathrm{c}\omega-\mathrm{d}-\mathrm{o}}$, ***(f)*** $G_{\mathrm{c}\omega-\mathrm{q}-\mathrm{o}}$

3.2 Tuning proportional–integral (PI) controllers

As shown in Fig. 1, the cascaded control loops are applied to the PMSG model in Simulink. In the inner control loop, duty ratios d_d and d_q are controlled by currents i_{Ld} and i_{Lq}. However, current i_{Lq} is controlled by the PMSG mechanical speed ω_{m} in the outer control loop. Tuning PI controllers for the current loops are not so difficult since the behaviour of the transfer functions $G_{\mathrm{cL\text{-}dd\text{-}o}}$ and $G_{\mathrm{cL\text{-}qq\text{-}o}}$ is almost identical within the same operating frequencies. The control loops are improved by adding a zero around the resonance frequency, which is 13 Hz to increase the phase curve in higher frequencies. Furthermore, the gains are tuned with an inverted control signal to adjust the crossover frequencies around 300 Hz. However, the speed controller is tuned a hundred times slower than the inner ones with one zero at 0.1 Hz. The tuned PI controllers are (see (15)) . The bode plots of the tuned PI controllers along with their corresponding transfer functions are shown in Fig. 6. In addition, Fig. 7 presents the block diagram explanation of the transfer function G_{plant} used in the control loop of the generator speed.

3.3 FRA in cascaded control-loop

Similar to the open-loop transfer function, the closed-loop transfer functions are first calculated including the effect of cross-coupling as shown in the block diagram of Fig. 8. However, the load torque does not remain constant and generator speed is given as feedback. The closed-loop d- and q-current control loops that need to be verified are defined as [11] (see (16)) , where G_{delay} is the delay function—calculated by third-order Padé approximation—which puts the unit delay to the current loop gains by half of the switching period.

Furthermore, for the speed control loop, it needs to have the current controller loop gain in order to calculate the closed-loop transfer functions related to the speed. Thus, the current loop gain $\boldsymbol{G}_{\mathrm{close}}$ is defined as

$$\boldsymbol{G}_{\mathrm{close}} = \begin{bmatrix} G_{\mathrm{cL-dd-o}} & G_{\mathrm{cL-qd-o}} \\ G_{\mathrm{cL-dq-o}} & G_{\mathrm{cL-qq-o}} \end{bmatrix} \begin{bmatrix} G_{\mathrm{cd}} & 0 \\ 0 & G_{\mathrm{cq}} \end{bmatrix}. \tag{17}$$

Now the closed-loop transfer function matrix $\boldsymbol{G}_{\mathrm{c}-\omega}$ that takes part in the control of generator speed can be calculated from (14) and (17) as [12]

$$\begin{aligned} \boldsymbol{G}_{\mathrm{c}-\omega} = & \begin{bmatrix} G_{\mathrm{c}\omega-\mathrm{d}-\mathrm{o}} & G_{\mathrm{c}\omega-\mathrm{q}-\mathrm{o}} \\ 0 & 0 \end{bmatrix} \begin{bmatrix} G_{\mathrm{cd}} & 0 \\ 0 & G_{\mathrm{cq}} \end{bmatrix} \\ & - \begin{bmatrix} G_{\mathrm{c}\omega-\mathrm{d}-\mathrm{o}} & G_{\mathrm{c}\omega-\mathrm{q}-\mathrm{o}} \\ 0 & 0 \end{bmatrix} \begin{bmatrix} G_{\mathrm{cd}} & 0 \\ 0 & G_{\mathrm{cq}} \end{bmatrix} (\boldsymbol{I} + \boldsymbol{G}_{\mathrm{close}})^{-1} \boldsymbol{G}_{\mathrm{close}}. \end{aligned} \tag{18}$$

Current controllers	Speed controller
$k_{\mathrm{c}} = -10^{(23/20)}\mathrm{rad/(sA)},$	$k_{\omega} = -10^{(40/20)\mathrm{A}.}$

$$G_{\mathrm{cd}} = k_{\mathrm{c}} \frac{((s/(2\pi \cdot 13\,\mathrm{Hz})) + 1)}{s} 1/A, \quad G_{\omega} = k_{\omega} \frac{((s/(2\pi \cdot 0.1\,\mathrm{Hz})) + 1)}{s} \mathrm{A/(rad/s)}, \quad G_{\mathrm{cq}} = k_{\mathrm{c}} \frac{((s/(2\pi \cdot 13\,\mathrm{Hz})) + 1)}{s} 1/A\,. \tag{15}$$

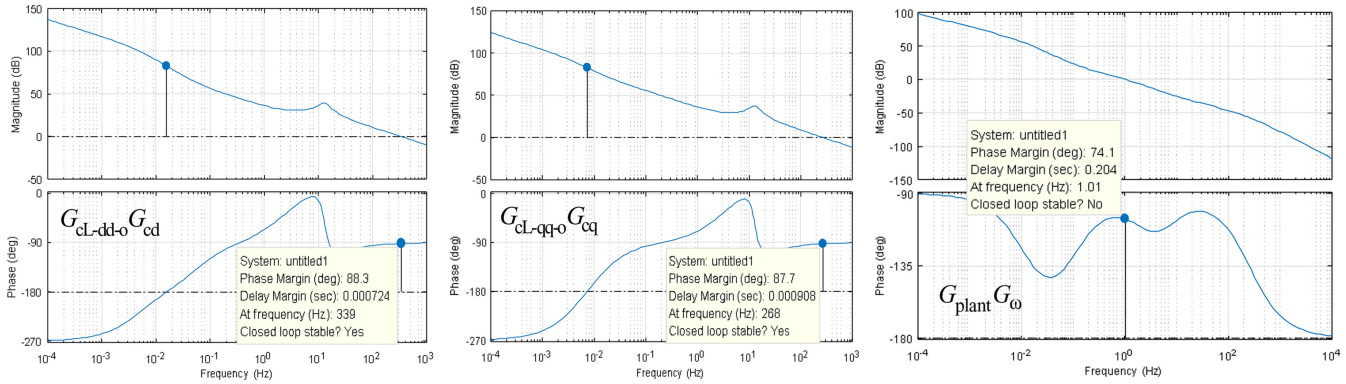

Fig. 6 *Bode plots of the tuned PI controllers and the corresponding transfer functions*

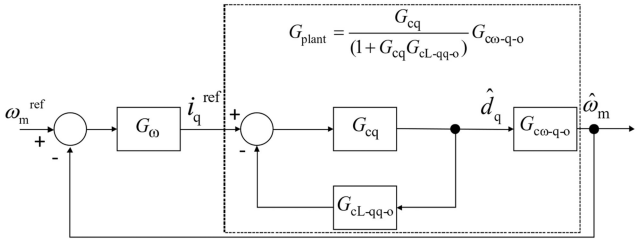

Fig. 7 *Block diagram of the transfer function G_{plant}*

$$\begin{cases} G_{\text{close}-d} = \dfrac{\hat{y}_{\text{loop}}}{\hat{u}_{\text{loop}}} = G_{cd}G_{\text{delay}}G_{cL-dd-o} - \dfrac{G_{cL-dq-o}G_{cL-qd-o}}{1+G_{cq}G_{cL-qq-o}}G_{cq}G_{cd}, \\ G_{\text{close}-q} = \dfrac{\hat{y}_{\text{loop}}}{\hat{u}_{\text{loop}}} = G_{cq}G_{\text{delay}}G_{cL-qq-o} - \dfrac{G_{cL-dq-o}G_{cL-qd-o}}{1+G_{cd}G_{cL-dd-o}}G_{cd}G_{cq}, \end{cases} \tag{16}$$

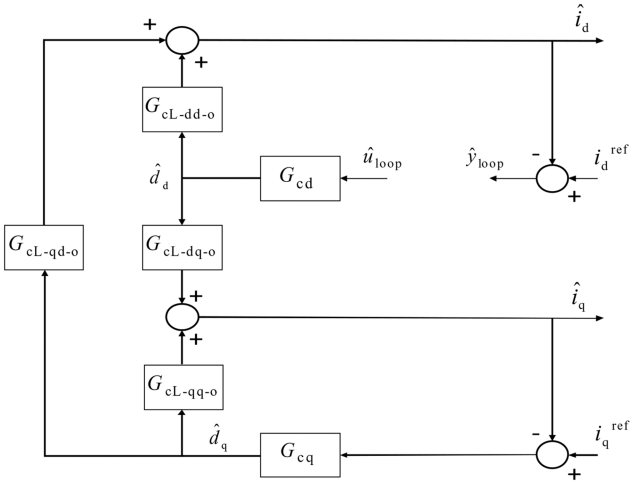

Fig. 8 *Control block diagram depicting the d-component current loop gain [11]*

The transfer function $G_{c-\omega}(1, 2)$ contributes to the speed controller loop gain $L_{\text{out}-\omega}$, which can be defined as

$$G_{\text{close}-\omega} = G_{c-\omega}(1,2)G_{\omega}. \tag{19}$$

The FRA verification results for the *d*- and *q*-current control loop gains and the speed loop gain are shown in Fig. 9. The dotted lines represent the calculated mathematical control loops and their corresponding frequency responses analysed using pseudo-random binary sequence (PRBS) in Simulink switched model are presented as solid lines in the graphs. In the PRBS method, a sinusoidal signal is injected to the input signal of the transfer function over a defined range of frequencies. The output signal of the transfer function is then measured.

3.4 Closed-loop stability performance

During steady-state, the closed-loop control stability of the PMSG and the rectifier model is tested by making step changes in the reference values of the inductor current *d*-component and the mechanical speed of the generator.

The generator *d*- and *q*-currents, mechanical speed and the load torque in response to the step changes of the reference values are shown in Fig. 10. The reference value of the *d*-axis current is varied from 0 to 10 A and then to −10 A, however, the mechanical speed reference is reduced to be half of its nominal value. As depicted in Fig. 10*a*, there is a small disturbance in the inductor *q*-current, however, the speed and torque respond oppositely in order to stabilise the system. In Fig. 10*b*, the torque should remain at its nominal value according to theory in response to change in reference speed, however, since the salient PMSG is controlled as non-salient that might be the reason of reduced load torque. In addition, there is an overshoot in the *d*- and *q*-currents and the load torque. The slow speed controller is one of the reasons for this overshoot.

4 Conclusion

In this study, the dynamic model of the wind turbine PMSG and the active rectifier is developed. In addition, the open-loop function and closed-loop transfer function are calculated and verified using frequency response analysis. The verification technique is proved to be an efficient tool in deterministic control design of cascaded current and speed control loops. Furthermore, the performance of the tuned PI controllers is tested by applying step changes in the reference values of the cascaded control loops in Simulink switched model. Hence, it can be concluded that the proposed verification technique can effectively participate in accurate control design of the wind turbine generator dynamics.

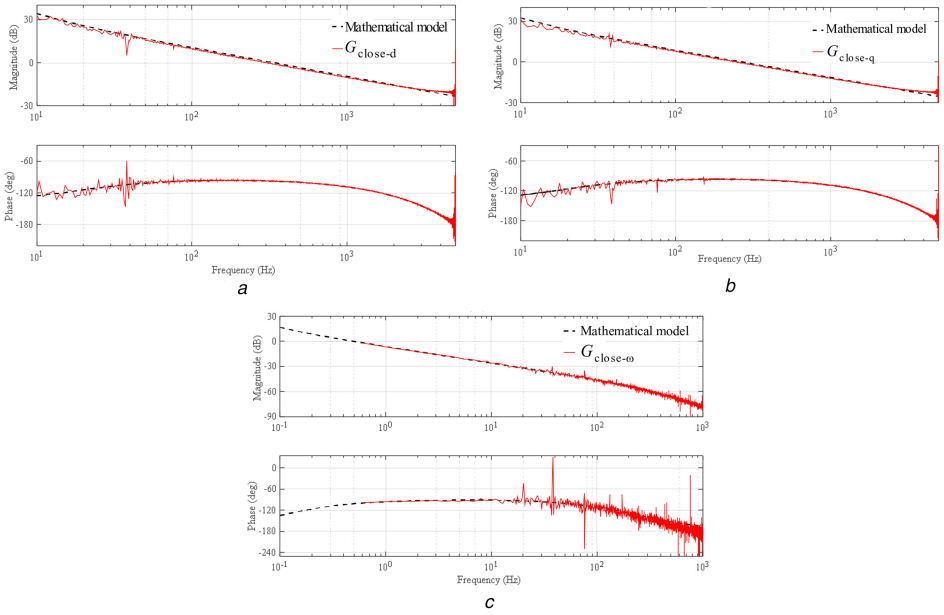

Fig. 9 *Frequency response analysis of closed-loop*
(a) $G_{\text{close-d}}$, ***(b)*** $G_{\text{close-q}}$, ***(c)*** $G_{\text{close}-\omega}$ using PRBS

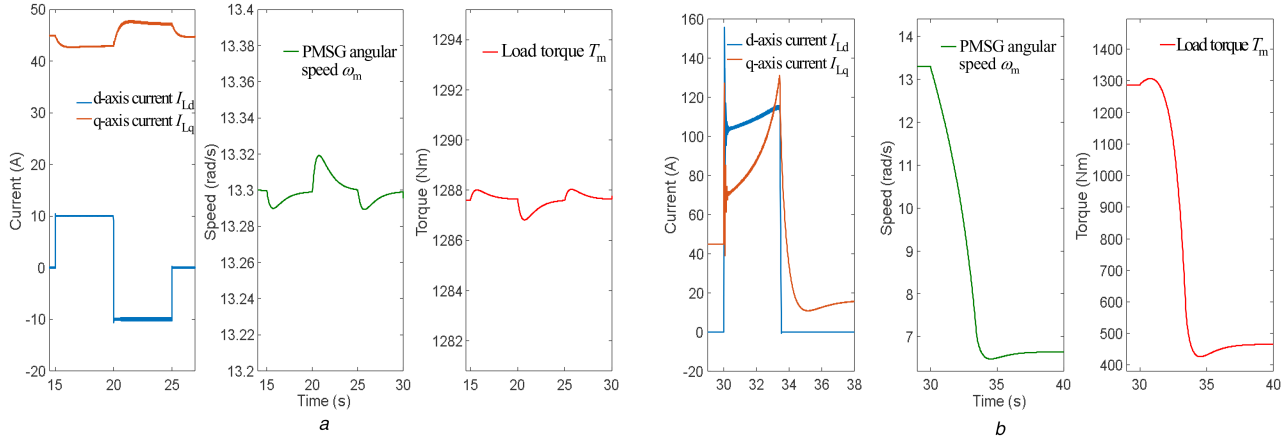

Fig. 10 *Steady-state stability performance of dq- generator currents I_{Ld}, I_{Lq}, load torque T_m and mechanical speed ω_m in response to the step change of*
(a) Inductor *d*-current from I_{Ld} and, ***(b)*** Mechanical speed ω_{m}

5 References

[1] Rolan, A., Luna, A., Vazquez, G., *et al.*: 'Modeling of a variable speed wind turbine with a permanent magnet synchronous generator'. Proc. Int. Symp. on Industrial Electronics, Seoul, South Korea, 2009

[2] Henckes, P., Knaut, A., Obermüller, F., *et al.*: 'The benefit of long-term high resolution wind data for electricity system analysis', *Energy*, 2018, **143**, pp. 934–942

[3] Koumba, P., Cheriti, A., Doumbia, M., *et al.*: 'Wind turbine control based on a permanent magnet synchronous generator connected to an isolated electrical network'. Proc. IEEE Electrical Power and Energy Conf. (EPEC), Saskatoon, Canada, 2017

[4] Yaramasu, V., Dekka, A., Durán, M., *et al.*: 'PMSG-based wind energy conversion systems: survey on power converters and controls', *IET Electr. Power Appl.*, 2017, **11**, pp. 956–968

[5] Korai, A., Rakhshani, E., Torres, J., *et al.*: 'Generic DSL-based modeling and control of wind turbine type 4 for EMT simulations in DIgSILENT power factory', in Gonzalez-Longatt, F., Rueda Torres, J.L. (Eds.): '*Advanced smart grid functionalities based on powerfactory*' (Springer, New York, NY, USA, 2018), pp. 355–371

[6] Guo, J., Lu, S., Zhai, C., *et al.*: 'Automatic bearing fault diagnosis of permanent magnet synchronous generators in wind turbines subjected to noise interference', *Meas. Sci. Technol.*, 2018, **29**, pp. 2–25

[7] Kocewiak, Ł., Álvarez, C.: 'Wind turbine harmonic model and its application overview, status and outline of the new IEC technical report'. 14th Int. Workshop Large-Scale Integration Wind Power into Power System and Transmission Networks Offshore Wind Power Plants, Brussels, Belgium, 2015

[8] Youssef, A., Mohamed, E., Ali, A.: 'Model predictive control for grid-tie wind-energy conversion system based PMSG'. Proc. Int. Conf. on Innovative Trends in Computer Engineering, Aswan Egypt, 2018

[9] Molina, M., Sanchez, A., Lede, A.: 'Dynamic modeling of wind farms with variable-speed direct-driven PMSG wind turbines'. Proc. IEEE/PES Transmission and Distribution Conf. and Exposition: Latin America (T&D-LA), Latin America, 2010

[10] Wu, B., Lang, Y., Zargari, N., *et al.*: '*Power conversion and control of wind energy systems*', vol. **76**, (John Wiley & Sons, Hoboken, NJ, USA, 2011)

[11] Suntio, T., Messo, T., Puukko, J.: '*Power electronic converters*' (Wiley, Weinheim, Germany, 2018)

[12] Aapro, A.: 'Factors in active damping design to mitigate grid interactions in three-phase grid-connected photovoltaic inverters'. PhD thesis, Tampere University of Technology, 2017